Selective Optimal Under-Frequency Load Shedding Based on Trajectory Sensitivities

A. Reveles-Pinedo
UNAM
Mexico City, México
ARevelesP@iingen.unam.mx

C.R. Fuerte-Esquivel
Universidad Michoacana
Morelia, México
claudio.fuerte@umich.mx

A. Pizano-Martínez
Universidad de Guanajuato
Salamanca, México
apizano@ugto.mx

R. Ramírez-Betancour
UJAT
Villahermosa, México
reymundo.ramirez@ujat.mx

***Abstract*—This paper proposes an optimal selective under-frequency load shedding strategy to perform a corrective control action that prevents the loss of frequency stability. The proposal decomposes this optimal load shedding problem into two mutually connected subproblems: the frequency stability analysis and the optimal load shedding. These two subproblems are sequentially solved until the minimum load shedding needed to recover the center-of-inertia frequency close to its nominal value is determined. The link between those two subproblems is a frequency performance index, which indicates the frequency deviation at each generation node with respect to the nominal frequency value. To selectively perform the load shedding, two novel methods are developed to identify which nodal loads most affect the frequency dynamics and to determine how the selected loads must be shed to return the frequency close to its nominal value at the maximum rate of change. The effectiveness of the proposed method is numerically demonstrated in two benchmark power systems.**

***Index Terms*—Directional derivative, event-driven, load shedding, frequency stability.**

NOMENCLATURE

FU	Frequency unstable
FS	Frequency stable
LFU	Last frequency unstable
FFS	First frequency stable
OP	System operating point
$\boldsymbol{LL}$	System's last loadability
$\boldsymbol{P}_d$	Active power demand
$\boldsymbol{Q}_d$	Reactive power demand
$\Delta\boldsymbol{P}_d$	Active power load shedding
$\Delta\boldsymbol{Q}_d$	Reactive power load shedding
$\Delta\boldsymbol{LL}$	Load shedding
f_i	Frequency at the *i*-th generator's node
f_n	Nominal frequency
f_{COI}	Center of inertia frequency
f_{PI}	Frequency performance index
$f_{PI,\,P_{di}}$	Frequency performance index at the *i*-th system loadability
∇f_{PI}	Gradient vector of the frequency performance index
H_i	Constant of inertia of the *i*-th generator
P_{di}^a	Load shedding availability at the *i*-th node
$\Delta\boldsymbol{P}_R$	Reference load shedding
$\Delta\boldsymbol{P}_{RD}$	Load shedding reference direction
ΔP_{RM}	Load shedding reference magnitude
p_{zi}, q_{zi}	Constant impedance portion of the load
p_{ci}, q_{ci}	Constant current portion of the load
p_{pi}, q_{qi}	Constant power portion of the load
k_{pi}, k_{qi}	Frequency characteristic coefficients
t_0	Time of fault inception
t_{cl}	Fault clearing time
t_{LS}	Time of load shedding application
t_{end}	Study time period
t_u	Time to instability
t_{nss}	Time to new steady-state

I. INTRODUCTION

The design of practical control actions to maintain the system's frequency dynamic response within bounds when a severe disturbance occurs in the electric power system is of paramount importance. In this vein, under-frequency load shedding (UFLS) schemes are used as the last resort to guarantee the system's frequency stability, defined as "the ability of a power system to maintain steady frequency following a severe system upset resulting in a significant imbalance between generation and load" [1]. In general, these schemes are classified into two categories: response-driven (RD) and event-driven (ED) UFLS [2], with the latter scheme being the most widely employed in practice [3]. In the RD-UFLS, the load shedding (LS) is triggered based on the system's transient response following a disturbance [4], [5], which involves the real-time monitoring of predefined electric state variables. Therefore, these schemes are executed in multiple steps to gradually retain the frequency stability and avoid over-shedding. By contrast, in the ED-UFLS schemes, the control actions are designed off-line, and they are automatically triggered following the occurrence of a contingency scenario without considering the feedback of the

system's transient response [2], [3]. Because the magnitude of the disturbance is known in advance, event-driven schemes tend to respond faster in critical situations [2], [3].

One aspect to address in the design of a UFLS scheme is how to determine the location and quantity of load to be shed. To achieve this goal, there are three general methods: load hierarchy-based classification [6], [7], a rate of change computation for a specific parameter with respect to (w.r.t.) the perturbation of nodal loads [8], [9] and the application of dynamic trajectory sensitivities [2], [10]. Regarding the latter, an optimal event-driven load shedding is proposed in [2] that simultaneously considers transients related to rotor angles, voltage magnitudes and frequency. Margin indices for these three types of transient behaviors are derived from time domain simulations to construct transient security and stability constraints, where the former set of constraints is associated with the transient voltage and frequency deviations. The LS is performed in two steps. First, a LS is determined to obtain a transiently stable operating point regarding rotor angles. This LS is considered the lower bound of a LS vector to stabilize possible voltage and frequency instability problems through a constrained optimization model that minimizes the cost of LS. On the other hand, an event-driven UFLS is proposed in [10], where the optimal LS is determined by minimizing the cost of nodal load shedding subject to a set of constraints, which include frequency dynamic approximations. These approximations are expressed in terms of frequency trajectory sensitivities of the system's frequency w.r.t. the amount of LS.

Based on the preceding discussion, a completely different frequency stability-constrained optimal load shedding (FSC-OLS) approach is proposed in this paper to determine how the LS must be optimally performed to avoid a post-fault loss of frequency stability. The proposed ED-UFLS approach relies on decomposing the FSC-OLS problem into two mutually connected subproblems: one associated with the frequency stability assessment (FSA) and the other related to the optimal selection of nodal LS. These two subproblems are sequentially solved until the minimum LS needed to retain the system stability is determined. The connection between both subproblems is achieved through a frequency performance index (FREPI) obtained from the FSA. The specific contributions of this work can be summarized below.

- A novel method for identifying the electric loads that have more impact on the stabilization of the post-fault dynamics of nodal frequencies is proposed based on the concepts associated with both the gradient of multivariable functions and trajectory sensitivity analysis.
- An original approach based on directional derivatives is proposed to determine how the direction and magnitude of nodal loads must change in the parametric load space to maintain the post-disturbance frequency stability.
- A new sequential formulation of the FSC-OLS problem is proposed to optimally perform a selective LS, which avoids heuristic decision techniques.

II. Fundamentals of the Frequency Control Approach

Considering an electric transmission system composed of a set of nodes $\mathcal{N} := \{1, 2, \ldots, N\}$ and a set of load nodes $\mathcal{N}_L := \{1, 2, \ldots, N_L\}$ such that $\mathcal{N}_L \subset \mathcal{N}$, the proposed approach's main objective is to optimally calculate the amount of LS that must be applied to a base load level, which defines the system's base operating point, to maintain the system's frequency within scheduled bounds for a specified contingency scenario. To achieve this objective, the proposed stabilization process is decomposed into two mutually connected problems: one related to the assessment of the system's frequency response for a given contingency scenario and the other associated with determining an optimal LS that bounds the system's frequency evolution within a secure region for that specified contingency. These two problems are sequentially solved until obtaining the LS at which the system's base operating point is declared a frequency stable equilibrium point because the deviation of generators' frequency is within specified bounds. In this frequency stabilization process, the information supplied from the frequency stability study to the optimization problem is the FREPI's sensitivities caused by perturbations of nodal loads and the resulting nodal load of active power after applying the LS. On the other hand, the information exchanged in the opposite direction is the nodal LS of active power that must be applied at a specified time in a new frequency stability study.

III. Frequency Stability Assessment

A. Frequency Stability Analysis

The frequency stability assessment (FSA) of a power system is assessed by solving the set of nonlinear differential-algebraic equations (DAEs) given by

$$\begin{aligned} \dot{\boldsymbol{x}} &= \boldsymbol{f}(\boldsymbol{x}, \boldsymbol{y}, \boldsymbol{\beta}) & \boldsymbol{f} &: \Re^{m+n+p} \to \Re^{m} \\ \boldsymbol{0} &= \boldsymbol{g}(\boldsymbol{x}, \boldsymbol{y}, \boldsymbol{\beta}) & \boldsymbol{g} &: \Re^{m+n+p} \to \Re^{n} \\ \boldsymbol{x} &\in \boldsymbol{X} \subset \Re^{m} \quad \boldsymbol{y} \in \boldsymbol{Y} \subset \Re^{n} \quad \boldsymbol{\beta} \in \boldsymbol{B} \subset \Re^{p} \end{aligned} \quad . \tag{1}$$

The dynamic variables of generators and controllers are contained in $\boldsymbol{x}$, while the algebraic variables are grouped in $\boldsymbol{y}$. Furthermore, $\boldsymbol{\beta}$ contains the system and operating parameters. The set of functions $\boldsymbol{f}(\cdot) = \boldsymbol{f}(\boldsymbol{x}, \boldsymbol{y}, \boldsymbol{\beta})$ represents the time evolution of dynamic variables, which are constrained to the set of nonlinear algebraic equations $\boldsymbol{g}(\cdot) = \boldsymbol{g}(\boldsymbol{x}, \boldsymbol{y}, \boldsymbol{\beta})$ that represent nodal power mismatches.

During the *k*-th iteration of the frequency stabilization process, the solution of (1) is performed for a period of time

Submitted to the 23rd Power Systems Computation Conference (PSCC 2024).

given by $T=[t_0,t_{cl}]\cup(t_{cl},t_{LS}]\cup(t_{LS},t_{end}]$ from an equilibrium point defined by the system's last loadability ($\boldsymbol{LL}$): OP^k($\boldsymbol{LL}^{k\text{-}1}$), where $\boldsymbol{LL}^{k-1}=\boldsymbol{P}_d^{k-1}+j\boldsymbol{Q}_d^{k-1}$. Furthermore, t_0 is the time at which the fault is incepted, t_{cl} denotes the fault clearing time and t_{LS} is the time at which the LS is applied. Finally, t_{end} is the study time period. Note that t_{cl} is null for outages of generators because the fault is not cleared.

Lastly, the active and reactive powers demanded at the i-th node at the t-th discrete time step of the solution of (1) are given by the sets of equations (2) or (3):

$$\begin{aligned}
P_{di}^{t,k} &= P_{di}^{t_0,k-1}\left(p_{zi}\left(V_i^{t,k}/V_i^{t_0^-}\right)^2+p_{ci}V_i^{t,k}/V_i^{t_0^-}+p_{pi}\right)\left(1+k_{pi}\Delta f^{t,k}\right)\\
Q_{di}^{t,k} &= Q_{di}^{t_0,k-1}\left(q_{zi}\left(V_i^{t,k}/V_i^{t_0^-}\right)^2+q_{ci}V_i^{t,k}/V_i^{t_0^-}+q_{qi}\right)\left(1+k_{qi}\Delta f^{t,k}\right)\\
&\forall t\in[t_0,t_{cl})\cup[t_{cl},t_{LS}),\ \ \forall i\in\mathcal{N}_L
\end{aligned}\tag{2}$$

$$\begin{aligned}
P_{di}^{t,k} &= P_{di}^{t_{LS},k-1}\left(p_{zi}\left(V_i^{t,k}/V_i^{t_0^-}\right)^2+p_{ci}V_i^{t,k}/V_i^{t_0^-}+p_{pi}\right)\left(1+k_{pi}\Delta f^{t,k}\right)\\
Q_{di}^{t,k} &= Q_{di}^{t_{LS},k-1}\left(q_{zi}\left(V_i^{t,k}/V_i^{t_0^-}\right)^2+q_{ci}V_i^{t,k}/V_i^{t_0^-}+q_{qi}\right)\left(1+k_{qi}\Delta f^{t,k}\right)\\
&\forall t\in[t_{LS},t_{end}],\ \ \forall i\in\mathcal{N}_L\ .
\end{aligned}\tag{3}$$

The set of equations (2) represent the voltage- and frequency-dependent ZIP-based load models [11]. In contrast, the set of equations (3) corresponds to equations (2) but considers the power demand after a load shedding has been performed, as indicated in the time periods associated with both sets of equations.

In (2) and (3), k_{pi} and k_{qi} denote the frequency characteristic coefficients. On the other hand, the amount of total load proportional to constant impedance, constant current and constant power is given by (p_{zi}, q_{zi}), (p_{ci}, q_{ci}) and (p_{pi}, q_{qi}), respectively. Lastly, $P_{di}^{t_{LS},k-1}$ and $Q_{di}^{t_{LS},k-1}$ are given by (4), where ΔP_{di}^{k-1} is the LS computed through the optimization process detailed in Section IV:

$$P_{di}^{t_{LS},k-1}=P_{di}^{t_0,k-1}-\Delta P_{di}^{k-1}\ ,\ Q_{di}^{t_{LS},k-1}=Q_{di}^{t_0,k-1}-\Delta P_{di}^{k-1}Q_{di}^{base}/P_{di}^{base}\ .\tag{4}$$

During the post-fault period, the possible violation of a frequency threshold is assessed at each discrete time step $t,\forall t>t_0$, through the deviation of each i-th machine's nodal frequency $f_i^k(t)$ from the nominal operating frequency f_n. The system frequency is declared insecure if the following inequality constraint is satisfied at a given time t_u, where N_g denotes the number of generators embedded in the network:

$$\left(f_n-f_i^k(t_u)\right)>\Delta f_{\max},\ i=1,\ldots,N_g\ .\tag{5}$$

Additionally, the solution of (1) at t_u permits quantifying how much the nodal frequency trajectories have deviated from the nominal frequency by defining a FREPI $f_{PI}(t_u)$, which is given by the sum of squared residuals:

$$f_{PI}^k(t_u)=\sum_{i=1}^{Ng}\left(f_n-f_i^k(t_u)\right)^2\ .\tag{6}$$

Note that a large value of $f_{PI}^k(t_u)$ indicates a large deviation of nodal frequency trajectories from f_n such that the FREPI's value must be reduced to avoid the condition (5).

Lastly, after applying the LS at t_{LS}, the power system will have another loadability given by $\boldsymbol{LL}^k=\boldsymbol{LL}^{k-1}-\Delta\boldsymbol{LL}^{k-1}$, which is referred to as a frequency unstable load level $\boldsymbol{LL}^{FU}$ if the OP^k is frequency unstable; otherwise, the resulting system's load is referred to as a frequency stable load level, which is denoted by $\boldsymbol{LL}^{FS}$.

B. Trajectory Sensitivity Analysis

If the frequency stability analysis declares the operating point OP^k($\boldsymbol{LL}^{k\text{-}1}$) as frequency unstable at time t_u, a way of judging the most influential loads in minimizing the value of $f_{PI}^k(t_u)$ is by computing how the time trajectory of $f_{PI}^k(t)$ changes for a small perturbation of each load $\left\{P_{di}^{t_0,k-1}\right\}_{i=1}^{N_L}$.

If the i-th load $P_{di}^{t_0,k-1}$ is slightly perturbed from $P_{di}^{t_0,k-1}$ to $\varepsilon P_{di}^{t_0,k-1}$, the numerical sensitivities of the nominal trajectory of $f_{PI}^k(t)$ (resp. $f_{COI}^k(t)$) w.r.t. changes in nodal loads correspond to the slope of the secant line through $f_{PI}^k\left(t,P_{di}^{t_0,k-1}\right)$ (resp. $f_{COI}^k\left(t,P_{di}^{t_0,k-1}\right)$) and the perturbed trajectory $f_{PI}^k\left(t,\varepsilon P_{di}^{t_0,k-1}\right)$ (resp. $f_{COI}^k\left(t,\varepsilon P_{di}^{t_0,k-1}\right)$). Hence, these dynamic trajectory sensitivities are given by [12]:

$$\frac{\partial f_{PI}^k(t)}{\partial P_{di}^{t_0,k-1}}\approx\frac{\delta f_{PI}^k(t)}{\delta P_{di}^{t_0,k-1}}\equiv\frac{f_{PI}^k\left(t,\varepsilon P_{di}^{t_0,k-1}\right)-f_{PI}^k\left(t,P_{di}^{t_0,k-1}\right)}{\varepsilon P_{di}^{t_0,k-1}-P_{di}^{t_0,k-1}},\tag{7}$$

$$\frac{\partial f_{COI}^k(t)}{\partial P_{di}^{t_0,k-1}}\approx\frac{\delta f_{COI}^k(t)}{\delta P_{di}^{t_0,k-1}}\equiv\frac{f_{COI}^k\left(t,\varepsilon P_{di}^{t_0,k-1}\right)-f_{COI}^k\left(t,P_{di}^{t_0,k-1}\right)}{\varepsilon P_{di}^{t_0,k-1}-P_{di}^{t_0,k-1}}.\tag{8}$$

Based on (7) and (8), it is possible to compute the gradient of $f_{PI}^k(t_u)$ w.r.t. changes in the system's COI frequency $f_{COI}^k(t_u)$, which in turn rises or falls as one changes nodal loads. Hence, if the i-th load $P_{di}^{t_0,k-1}$ has a small perturbation over its nominal value that results in $\varepsilon P_{di}^{t_0,k-1}$, the i-th element of the gradient vector $\nabla f_{PI}^k(t_u)$ corresponds to the sensitivity of $f_{PI}^k(t_u)$ w.r.t. to the change of $f_{COI}^k(t_u)$ produced by the perturbation of $P_{di}^{t_0,k-1}$:

$$\nabla f_{PI}^k(t_u)_i=\frac{f_{PI,\varepsilon P_{di}^{t_0,k-1}}^k(t_u)-f_{PI,P_{di}^{t_0,k-1}}^k(t_u)}{f_{COI,\varepsilon P_{di}^{t_0,k-1}}^k(t_u)-f_{COI,P_{di}^{t_0,k-1}}^k(t_u)}\quad\forall i\in\mathcal{N}_L\ ,\tag{9}$$

where $f^{k}_{PI,\,P^{t_0,k-1}_{di}}(t_u)$ is given by

$$f^{k}_{PI,\,P^{t_0,k-1}_{di}}(t_u)=\sum_{i=1}^{Ng}\left(f_n-f^{k}_{i,\,P^{t_0,k-1}_{di}}(t_u)\right)^2 . \quad (10)$$

Furthermore, the value of $f^{k}_{COI,P^{t_0,k-1}_{di}}(t_u)$ is given by (11), where H_i represents the inertia constant of the *i*-th generator:

$$f^{k}_{COI,P^{t_0,k-1}_{di}}(t_u)=\sum_{i=1}^{Ng}H_i f^{k}_{i,P^{t_0,k-1}_{di}}(t_u)\Big/\sum_{i=1}^{Ng}H_i . \quad (11)$$

Similarly, the values of $f^{k}_{PI,\,\varepsilon P^{t_0,k-1}_{di}}(t_u)$ $\forall i=1,\ldots,N_g$ and $f^{k}_{COI,\,\varepsilon P^{t_0,k-1}_{di}}(t_u)$ are also obtained by solving (1) for the period of time $T=[t_0,t_{cl}]\cup(t_{cl},t_{LS}]\cup(t_{LS},t_u]$ by considering each perturbation $\varepsilon P^{t_0,k-1}_{di}$ $\forall i=1,\ldots,N_L$ and the specified contingency scenario. Based on the results of this set of time domain simulations, $f^{k}_{PI,\,\varepsilon P^{t_0,k-1}_{di}}(t_u)$ and $f^{k}_{COI,\,\varepsilon P^{t_0,k-1}_{di}}(t_u)$ are computed by (10) and (11), respectively, by changing the subindex $P^{t_0,k-1}_{di}$ by $\varepsilon P^{t_0,k-1}_{di}$. Hence, the required sensitivities are directly obtained from the change in the dynamic trajectories of nodal frequencies caused by a small change in loads.

IV. Optimal Assessment of Load Shedding

If the FSA executed at the (*k*-1)-th iteration of the stabilization process detected that OP^{k-1}($\boldsymbol{LL}^{k-2}$) is a frequency unstable equilibrium point, the guiding principle for determining the vector of LS $\Delta\boldsymbol{LL}^{k-1}$ to be applied during the FSA at the *k*-th iteration is based on finding a suitable vector of active power LS $\Delta\boldsymbol{P}_d^{k-1}$ through the proposed frequency stability-constrained optimal LS (FSC-OLS) as follows. In the Euclidean space, the vector $\Delta\boldsymbol{P}_d^{k-1}$ is composed of the amount of active load to be shed at each node:

$$\Delta\boldsymbol{P}_d^{k-1}=\left[\Delta P_{d1}^{k-1},.....\Delta P_{d\,N_L}^{k-1}\right]^{\mathrm{T}} , \quad (12)$$

where T indicates a transposed vector. Once $\Delta\boldsymbol{P}_d^{k-1}$ is determined, the reactive power LS $\Delta\boldsymbol{Q}_d^{k-1}$ is directly computed by considering a constant power factor, which results in a known $\Delta\boldsymbol{LL}^{k-1}$.

The new LS $\Delta\boldsymbol{P}_d^{k-1}$ must be optimally computed based on the following information provided by the FSA: i) the vector of trajectory sensitivities $\nabla f^{k}_{PI}(t_u)$ and ii) the system's $\boldsymbol{LL}$ of active power load $\boldsymbol{P}_d^{k-1}$ with components $\left\{P_{di}^{k-1}\right\}_{i=1}^{N_L}=\left\{P_{di}^{t_0,k-1}-\Delta P_{di}^{k-1}\right\}_{i=1}^{N_L}$. Conversely, determining the suitable LS that avoids the post-fault loss of frequency stability requires decomposing $\Delta\boldsymbol{P}_d^{k-1}$ in terms of its magnitude $\Delta P_M^{k-1}=\left\|\Delta\boldsymbol{P}_d^{k-1}\right\|$ and a vector that points in the same reference direction as $\Delta\boldsymbol{P}_d^{k-1}$ with a length 1: the unit vector $\Delta\boldsymbol{P}_D^{k-1}=\Delta\hat{\boldsymbol{P}}_d^{k-1}=\Delta\boldsymbol{P}_d^{k-1}\big/\left\|\Delta\boldsymbol{P}_d^{k-1}\right\|$. The resulting equation is given by

$$\Delta\boldsymbol{P}_d^{k-1}=\Delta P_M^{k-1}\Delta\boldsymbol{P}_D^{k-1} . \quad (13)$$

In the context of the frequency stabilization process, if the magnitude ΔP_M^{k-1} and the direction $\Delta\boldsymbol{P}_D^{k-1}$ of the LS $\Delta\boldsymbol{P}_d^{k-1}$ are properly adjusted, the dynamic trajectories of frequencies will evolve towards a frequency stable region after the LS is performed. In order to accomplish the proper adjustment of $\Delta\boldsymbol{P}_d^{k-1}$, however, a reference magnitude ΔP_{RM}^{k-1} and reference direction $\Delta\boldsymbol{P}_{RD}^{k-1}$ must be properly assessed to steer the system's frequency response towards a frequency stable operating region. The assessment of these references is described below.

C. Estimation of the Reference Load Shedding

To perform the correct LS in the direction of the bounded frequency region, one must determine a reference active power LS: $\Delta\boldsymbol{P}_R^{k-1}$, defined by the direction and magnitude in which the nodal load profile must change in the parametric load space of active power. This section describes how to compute the reference direction $\Delta\boldsymbol{P}_{RD}^{k-1}$ and reference magnitude ΔP_{RM}^{k-1} associated with $\Delta\boldsymbol{P}_R^{k-1}$ at the (*k*-1)-th iteration of the stabilization process: $\Delta\boldsymbol{P}_R^{k-1}=\Delta P_{RM}^{k-1}\Delta\boldsymbol{P}_{RD}^{k-1}$.

1) Reference direction of load shedding $\Delta\boldsymbol{P}_{RD}$

Determining whether an active power load should increase or decrease its value to improve the system's frequency stability defines the reference direction of LS. The direction in which each nodal load must change in the parametric load space is grouped in the reference direction vector $\Delta\boldsymbol{P}_{RD}^{k-1}$. The components of $\Delta\boldsymbol{P}_{RD}^{k-1}$ are determined from the rate of change at which the value of $f_{PI}^{k-1}(t_u)$ decreases most rapidly because of perturbations in nodal loads.

The directional derivative of $f_{PI}^{k-1}(t_u)$ in the direction $\Delta\boldsymbol{P}_{RD}^{k-1}$ is given by the dot product of the vectors $\nabla f_{PI}^{k-1}(t_u)$ and $\Delta\boldsymbol{P}_{RD}^{k-1}$ as shown in (14), where ϕ is the angle between vectors $\nabla f_{PI}^{k-1}(t_u)$ and $\Delta\boldsymbol{P}_{RD}^{k-1}$. Hence, (14) represents the scalar projection of the gradient vector $\nabla f_{PI}^{k-1}(t_u)$ onto $\Delta\boldsymbol{P}_{RD}^{k-1}$:

$$\nabla f_{PI}^{k-1}(t_u)\bullet\Delta\boldsymbol{P}_{RD}^{k-1}=\sum_{i=1}^{N_L}\nabla f_{PI}^{k-1}(t_u)_i\Delta P_{RD\,i}^{k-1}=\left\|\nabla f_{PI}^{k-1}(t_u)\right\|\left\|\Delta\boldsymbol{P}_{RD}^{k-1}\right\|\cos\phi. \quad (14)$$

Since $\nabla f_{PI}^{k-1}(t_u)$ points in the direction of the fastest increase of $f_{PI}^{k-1}(t_u)$, the direction of the unit vector $\Delta\boldsymbol{P}_{RD}^{k-1}$

must be the opposite of $\nabla f_{PI}^{k-1}(t_u)$ to decrease $f_{PI}^{k-1}(t_u)$ most rapidly:

$$\Delta \boldsymbol{P}_{RD}^{k-1} = -\nabla f_{PI}^{k-1}(t_u) \Big/ \left\| \nabla f_{PI}^{k-1}(t_u) \right\|. \quad (15)$$

Lastly, note that the computation of $\Delta \boldsymbol{P}_{RD}^{k-1}$ by (15) indicates that the angle between vectors $\nabla f_{PI}^{k-1}(t_u)$ and $\Delta \boldsymbol{P}_{RD}^{k-1}$ is 180°: $\cos\phi$ equals -1, which results in the minimum value of the dot product (14).

The absolute value and sign of each component of $\Delta \boldsymbol{P}_{RD}^{k-1}$ provide valuable information about performing the LS for the frequency stabilization process. On the one hand, the components of $\Delta \boldsymbol{P}_{RD}^{k-1}: \left\{\Delta P_{RDi}^{k-1}\right\}_{i=1}^{N_L}$ with the higher absolute values correspond to the active power loads that improve the frequency stability most significantly. On the other hand, the negative components of $\Delta \boldsymbol{P}_{RD}^{k-1}$: $\left\{\Delta P_{RDi}^{k-1} < 0\right\}_{i=1}^{N_L}$, which are grouped in the subset of curtailed loads (*CL*), i.e., $\mathcal{N}_L^{CL} \subset \mathcal{N}_L$, correspond to the active power loads that must be curtailed to reduce the value of $f_{PI}^{k-1}(t_u)$ in order to steer the system to a frequency stable region. Finally, the positive components of $\Delta \boldsymbol{P}_{RD}^{k-1}$: $\left\{\Delta P_{RDi}^{k-1} \geq 0\right\}_{i=1}^{N_L}$, which compose the subset of non-curtailed loads (*NCL*), i.e., $\mathcal{N}_L^{NCL} \subset \mathcal{N}_L$, correspond to the active power loads that must be increased to reduce the value of $f_{PI}^{k-1}(t_u)$. Since the proposed approach focuses on UFLS, however, these loads remain fixed at their previous values during the iterative solution of the FSC-OLS optimization problem. Based on the information mentioned above, the loads to be curtailed can be selected in a non-heuristic way.

2) Reference magnitude of load shedding ΔP_{RM}

The reference magnitude ΔP_{RM}^{k-1} corresponds to the maximum amount of load curtailment to be performed in the reference direction $\Delta \boldsymbol{P}_{RD}^{k-1}$. To assess this reference magnitude, the optimization problem (16) to (18) must be first solved for the vector of maximum loadability of active power $\boldsymbol{P}_{d_{\max}}^{k}$ with components $\left\{P_{di_{\max}}^{k}\right\}_{i=1}^{N_L}$:

$$\min_{\boldsymbol{P}_{d_{\max}}^{k}} f(\cdot) = \left(-\left[\Delta \boldsymbol{P}_{RD}^{k-1} \right]^{\mathrm{T}} \bullet \left(\boldsymbol{P}_{d_{\max}}^{k} - \boldsymbol{P}_{d}^{k-1} \right) \right) \quad (16)$$

$$0 \leq P_{di_{\max}}^{k} \leq P_{di}^{k-1}, \ \forall i \in \mathcal{N}_L^{CL} \quad (17)$$

$$P_{di_{\max}}^{k} - P_{di}^{k-1} = 0, \ \forall i \in \mathcal{N}_L^{NCL}. \quad (18)$$

Once $\boldsymbol{P}_{d_{\max}}^{k}$ has been obtained, ΔP_{RM}^{k-1} is computed from the dot product of $\Delta \boldsymbol{P}_{RD}^{k-1}$ and the unit vector of $\boldsymbol{P}_{d_{\max}}^{k} - \boldsymbol{P}_{d}^{k-1}$.

D. FSC-OLS Model for Optimal Load Shedding

Based on the LS reference vector $\Delta \boldsymbol{P}_R^{k-1} = \Delta P_{RM}^{k-1} \Delta \boldsymbol{P}_{RD}^{k-1}$, the proposed FSC-OLS model is given in (19) to (21). Once the optimization problem is solved for the LS availability at each load node $\left\{P_{di}^{a,k}\right\}_{i=1}^{N_L}$, which are lumped together in $\boldsymbol{P}_d^{a,k}$, the vector of active power to be shed at each node is given by the Hadamard product $\Delta \boldsymbol{P}_d^{k-1} = \Delta \boldsymbol{P}_R^{k-1} \odot \left(\boldsymbol{P}_d^{a,k} - \boldsymbol{P}_d^{k-1} \right)$:

$$\min_{\boldsymbol{P}_d^{a,k}} \Delta P_d^{k-1} = \left(-\left[\Delta \boldsymbol{P}_R^{k-1} \right]^{\mathrm{T}} \bullet \left(\boldsymbol{P}_d^{a,k} - \boldsymbol{P}_d^{k-1} \right) \right), \quad (19)$$

$$0 \leq P_{di}^{a,k} \leq P_{di}^{k-1}, \ \forall i \in \mathcal{N}_L^{CL}, \quad (20)$$

$$P_{di}^{a,k} - P_{di}^{k-1} = 0, \ \forall i \in \mathcal{N}_L^{NCL}. \quad (21)$$

Lastly, the vector $\Delta \boldsymbol{P}_d^{k-1}$ is used to perform the LS during the FSA at the *k*-th iteration of the stabilization process through (4) for the active and reactive power loads.

V. FSC-OLS Stabilization Process

Considering a frequency unstable operating point OP^k for a selected contingency scenario and a loadability level $\boldsymbol{LL}^{k-1}$, the proposed stabilization algorithm consists of two phases: a) the bracketing and b) the refinement phases [13], which are described in detail below.

A. Bracketing Phase

At the *k*-th iteration of the bracketing phase, a FSA is performed by solving (1) for a given contingency scenario, a system's $\boldsymbol{LL}^{k-1}$ and a specified LS $\Delta \boldsymbol{LL}^{k-1} = \Delta \boldsymbol{P}_d^{k-1} + j \Delta \boldsymbol{Q}_d^{k-1}$. If the condition (5) is satisfied at t_u, the $OP^k(\boldsymbol{LL}^{k-1})$ is declared unstable, and the trajectory sensitivity analysis of $f_{PI}(t_u)$ is performed to obtain the numerical sensitivities given by (7) and (8). Based on the gradient vector $\nabla f_{PI}^{k}(t_u)$, the reference direction $\Delta \boldsymbol{P}_{RD}^{k}$ and the reference magnitude ΔP_{RM}^{k} are computed from (15) and the optimization problem (16) to (18), respectively. An optimal LS $\Delta \boldsymbol{P}_d^{k}$ is then obtained by solving the constrained optimization problem (19) to (21). Lastly, $\Delta \boldsymbol{LL}^{k} = \Delta \boldsymbol{P}_d^{k} + j \Delta \boldsymbol{Q}_d^{k}$ is computed by using $\Delta \boldsymbol{P}_d^{k}$ to determine the amount of reactive power to be shed: $\Delta \boldsymbol{Q}_d^{k}$, where

$$\left\{\Delta Q_{di}^{k}\right\}_{i=1}^{N_L} = \left\{ \left(Q_{di}^{base} / P_{di}^{base} \right) \Delta P_{di}^{k} \right\}_{i=1}^{N_L}. \quad (22)$$

This stabilization process is repeated by performing a new (*k*+1)-th iteration of the bracketing phase until obtaining a LS $\Delta \boldsymbol{P}_d^{k_{final}}$ in the k_{final}-th iteration in which the operating point $OP^{k_{final}+1}(\boldsymbol{LL}^{k_{final}})$ withstands the contingency scenario in terms of recovering the steady-state frequency value above a specified threshold: $\left(f_i^{k_{final}}(t_{end}) - f_n \right) > \Delta f_{\max}^{BS}$, $i = 1, \ldots, N_g$.

Lastly, once $\Delta \boldsymbol{P}_d^{k_{final}}$ has been found, the total amount of LS $\Delta \boldsymbol{LS}^{total}$ to be applied to the base operating point OP^{base} at t_{LS} is given by $\Delta \boldsymbol{LS}^{total} = \sum_{i=1}^{k_{final}} \Delta \boldsymbol{LL}^i$.

Based on the information mentioned above, the bracketing phase is outlined in Figure 1.

B. Refinement Phase

The refinement stage is activated if and only if $\left(f_i^{k_{final}}(t_{end}) - f_n \right) > \Delta f_{\max}^{RS},\ i = 1, \ldots, N_g$, where $\Delta f_{\max}^{RS} < \Delta f_{\max}^{BS}$. The activation constraint implies that in the solution of the bracketing phase the frequency evolution does not stabilize to a value near the nominal frequency. In this case, after obtaining the first frequency stable operating point OP^{FFS} from the bracketing phase, the results transferred to the refinement phase are the last reference direction and magnitude computed at the bracketing phase: $\Delta \boldsymbol{P}_{RD}^{LFU}$, ΔP_{RM}^{LFU} and the base active power demanded at each node $\boldsymbol{P}_d^{base}$. Furthermore, the interval T_M at the *k*-th iteration of this stage is defined in terms of the reference magnitude of LS in order to apply the bisection process: $T_M = \left[\Delta P_{RM\_low}^k = 0, \Delta P_{RM\_up}^k = \Delta P_{RM}^{LFU} \right]$.

Based on the data mentioned above, the refinement phase changes the total amount of active power shedding $\Delta \boldsymbol{P}_d^{total}$ applied to $\boldsymbol{P}_d^{base}$ in the reference direction $\Delta \boldsymbol{P}_{RD}^{LFU}$ to steer the evolutions of generators' nodal frequencies and thus the COI frequency toward a value close to the nominal frequency. This goal is achieved by iteratively adjusting the reference magnitude ΔP_{RM} by considering the vectors $\Delta \boldsymbol{P}_{RD}^{LFU}$ and $\boldsymbol{P}_d^{base}$ as references, which remain fixed during the refinement phase. At the *k*-th iteration of the refinement phase, a new reference magnitude is computed by bisecting the interval T_M : $\Delta P_{RM}^k = \left(\Delta P_{RM\_low}^k + \Delta P_{RM\_up}^k \right) / 2$. Based on this new value of ΔP_{RM}^k and the known vectors $\Delta \boldsymbol{P}_{RD}^{LFU}$ and $\boldsymbol{P}_d^{base}$, the FSC-OLS problem given by (19) to (21) is solved to obtain an optimal active LS $\Delta \boldsymbol{P}_d^k$ with components that are used to compute the system's new loadability through (4) when applying the LS during the FSA of OP^{base}. Note that the trajectory sensitivity analysis is not required during the FSA at this refinement stage. If this analysis detects that nodal frequency evolutions at generators' nodes satisfy $\left(f_i^k(t_{end}) - f_n \right) > TOL,\ i = 1, \ldots, N_g$, the upper endpoint of T_M must change to $\Delta P_{RM\_up}^k = \Delta P_{RM}^k$. On the other hand, if $\left(f_n - f_i^k(t_{end}) \right) > TOL,\ i = 1, \ldots, N_g$, the lower endpoint of T_M is the one changed to $\Delta P_{RM\_low}^k = \Delta P_{RM}^k$. For the purpose of simulations *TOL*= $\Delta f_{\max}^{RS}$. This iterative process continues until the constraints mentioned above are no longer violated. Lastly, the procedure described above is schematically shown in Figure 2.

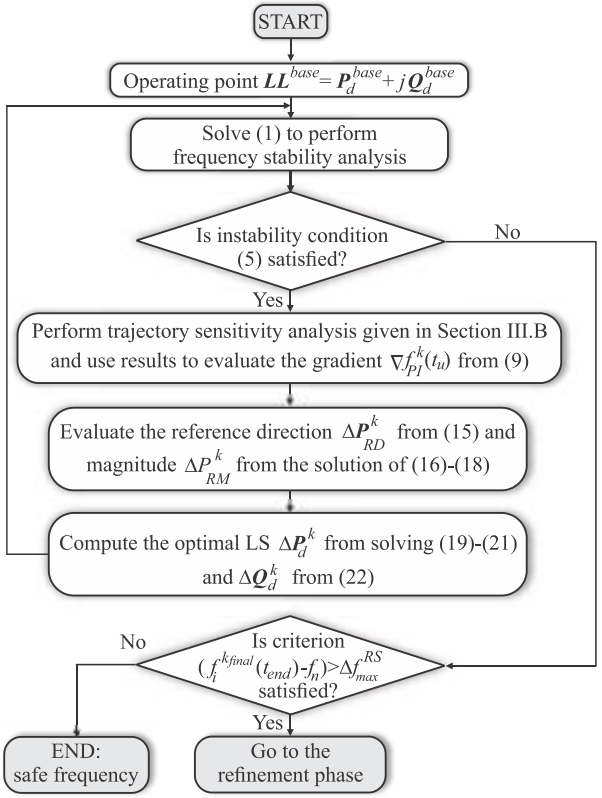

Figure 1. Bracketing phase of the FSC-OLS stabilization process.

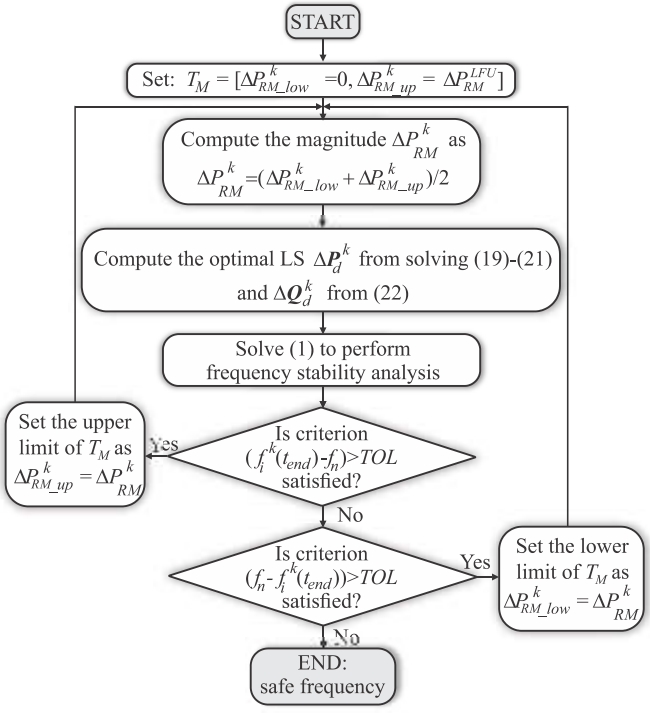

Figure 2. Refinement phase of the FSC-OLS stabilization process.

VI. CASE STUDIES

By applying the proposed OLS approach, the frequency control is numerically demonstrated in this Section. Two case studies are reported considering the New England 39-bus system and the IEEE 118-bus system, respectively. All loads are modeled with the voltage and frequency dependent model given in (2) and (3), with polynomial coefficients given as $p_{pi}=q_{qi}=0.4$, $p_{ci}=q_{ci}=0.4$, $p_{zi}=q_{zi}=0.2$ [14] and $k_{pi}=k_{qi}=1$ [11]. On the other hand, the generators are represented by the sixth order model, while their corresponding control units consist of an IEEE type 1 exciter and a single reheat tandem-compound steam turbine governor model. Lastly, the transient safety assessment tool (TSAT), included in the DSATools™ software [15], is used to perform dynamic simulations that provide the evolutions of nodal frequencies when the system is subjected to a contingency scenario.

C. New England 39-bus system

The New England 10-machine, 19-load, 39-bus system data for the dynamic- and steady-state analyses are taken from [16]. The contingency consists of a generator trip event incepted at t_0 =10s at bus 30, which provokes the loss of 250 MWs: a 4.45% of the total system's generation of active power. Under this contingency scenario, the COI frequency computed by (11) decays to a steady-state value of 59.53 Hz if no LS is applied, as shown in Figure 3.

By considering the setpoint of 59.7 Hz for activating the first UFLS step used in the Florida Reliability Coordinating Council (FRCC) scheme [17], the maximum allowed nodal frequency deviation of Δf_{max}=0.3 Hz is employed in (5), from which the first under-frequency relay is activated. In addition, a value of $\Delta f_{\max}^{BS} = 0.2$ Hz is considered in the bracketing phase to reestablish the nodal frequencies at generators' nodes above the threshold of Δf_{max}. Lastly, the steady-state value of the frequency to be obtained in the refinement phase is defined close to its nominal value by assuming $\Delta f_{\max}^{RS} = 0.1$ Hz.

Based on the information mentioned above, the TD simulation detects the violation of Δf_{max} at t_u=14s with a value of $f_{PI}(t_u)$=0.8281Hz, which triggers the frequency stabilization process through the computation of dynamic sensitivities and the reference values of $\Delta \boldsymbol{P}_{RD}^1$ and ΔP_{RM}^1 at the bracketing stage. The reference direction vector $\Delta \boldsymbol{P}_{RD}^1$ is shown in Table I for each nodal load, where it is clear that only 15 loads must be shed. Furthermore, the reference magnitude ΔP_{RM}^1 has a value of 0.3135. The reference vector of LS $\Delta \boldsymbol{P}_R^1$ is then computed and used in the OLS problem to obtain the first optimal LS that corresponds to a total amount of 372 MWs, with nodal load sheds of active power defined by the vector $\Delta \boldsymbol{P}_d^1$, as indicated in Table II. Finally, $\Delta \boldsymbol{LL}^1 = \Delta \boldsymbol{P}_d^1 + j\Delta \boldsymbol{Q}_d^1$ is computed to perform a new FSA where the LS of $\Delta \boldsymbol{LL}^1$ is applied at t_u. This second FSA indicates that the COI frequency increased from 59.7 Hz to about 60.15 Hz. Since the COI frequency above 59.8 Hz was achieved based on an over shedding, the amount of LS must be reduced by applying the refinement stage of the proposed approach. In this last stage of the stabilization process, the resulting total amount of LS was 192.85 MW with the amount of active power load to be shed at each node, as reported in Table III. Hence, only 3.16% of the total load was disconnected to stabilize the generators' nodal frequencies and to return the COI frequency to a value of 59.90 Hz, as shown in Figure 3.

TABLE I. $\Delta \boldsymbol{P}_{RD}$ values of loads

Bus	$\Delta \boldsymbol{P}_{RD}$	Bus	$\Delta \boldsymbol{P}_{RD}$	Bus	$\Delta \boldsymbol{P}_{RD}$	Bus	$\Delta \boldsymbol{P}_{RD}$
3	-0.1342	15	-0.1355	23	-0.1933	28	-0.2289
4	**0.0094**	16	-0.1285	24	-0.1447	29	-0.1681
7	-0.2034	18	-0.2643	25	-0.2161	31	-0.3774
8	**0.0260**	20	**0.0977**	26	-0.2802	39	**0.4661**
12	-0.3789	21	-0.1722	27	-0.1688		

TABLE II. Nodal load shedding at the first iteration of the bracketing phase

Bus	ΔP (MW)	% of P_d	Bus	ΔP (MW)	% of P_d
3	27.08	8.41%	23	30.00	12.12%
4	0.00	0.00%	24	28.00	9.07%
7	29.70	12.75%	25	30.35	13.55%
8	0.00	0.00%	26	24.42	17.57%
12	1.78	23.73%	27	29.74	10.58%
15	27.18	8.49%	28	29.56	14.35%
16	26.51	8.06%	29	29.88	10.54%
18	26.18	16.57%	31	2.18	23.70%
20	0.00	0.00%	39	0.00	0.00%
21	29.59	10.80%	**Total**	**372.15**	**6.10%**

TABLE III. Final nodal load shedding

Bus	ΔP (MW)	% of P_d	Bus	ΔP (MW)	% of P_d
3	13.55	4.21%	23	6.44	7.90%
4	0.00	0.00%	24	4.61	5.76%
7	16.16	6.94%	25	7.37	8.96%
8	0.00	0.00%	26	9.32	11.70%
12	0.00	0.00%	27	5.58	6.82%
15	13.62	4.26%	28	7.76	9.47%
16	13.03	3.96%	29	5.50	6.85%
18	14.10	8.92%	31	0.00	16.09%
20	0.00	0.00%	39	0.00	0.00%
21	15.54	5.67%	**Total**	**192.85**	**3.16%**

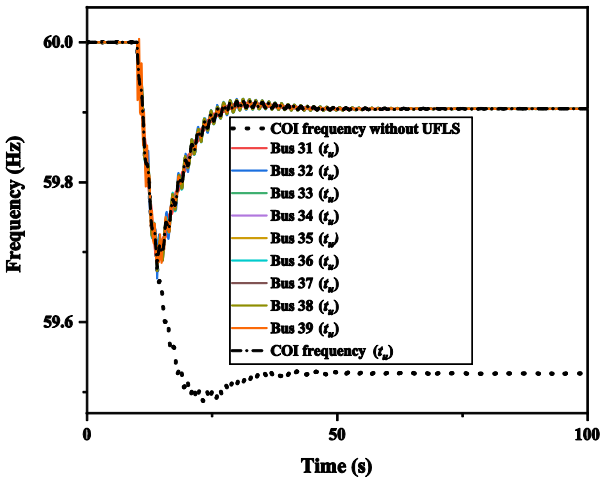

Figure 3. Frequencies for the New England 39-bus system for LS at t_u.

TABLE IV. Nodal load shedding with t_{nss}=100s

Bus	ΔP (MW)	% of P_d	Bus	ΔP (MW)	% of P_d
3	17.00	5.28%	23	19.56	7.90%
4	0.00	0.00%	24	17.77	5.76%
7	19.60	8.41%	25	20.06	8.96%
8	0.00	0.00%	26	16.26	11.70%
12	1.21	16.13%	27	19.17	6.82%
15	17.12	5.35%	28	19.50	9.47%
16	16.59	5.04%	29	19.43	6.85%
18	17.39	11.01%	31	1.48	16.09%
20	0.00	0.00%	39	0.00	0.00%
21	19.10	6.97%	**Total**	**241.24**	**3.96%**

TABLE V. Comparison of UFLS schemes

UFLS Scheme	Frequency value (Hz)	ΔP (MW)	% of total P_d
Proposed approach	59.99	241.24	3.96%
UFLS [9]	60.19	491.40	8.06%
FRCC UFLS [17]	60.12	548.67	9.00%

TABLE VI. CPU time for the frequency stabilization (in seconds)

Stage	Frequency analysis		FSC-OLS phase		Total
	Stability	Sensitivity	Bracketing	Refinement	
Time	2.06	53.63	10.18	6.64	72.51

A more efficient LS that increases the nodal frequencies to a value very close to the nominal value is recommended in [18], where the UFLS scheme is designed based on the maximum load-generation imbalance that is obtained once the frequency settles at its minimum value after the contingency. Within the context of the proposed approach, this idea is implemented by computing the dynamic sensitivities at time t_{nss}, instead of t_u, at which the frequency evolution has reached a new steady-state value.

The case study described above was repeated by computing the dynamic sensitivites at t_{nss}=100s and by applying the LS at t_u =14s. In this case, the same 15 loads had to be shed during the stabilization process that required a single iteration in the bracketing phase and two iterations in the refinement stage. The solution of the stabilization process determined a total of 241.24 MWs to be shed, as reported in Table IV, to recover the nodal frequencies and COI frequency up to a value of 59.99 Hz, as shown in Figure 4.

The LS obtained with the proposed approach is now compared with the total amount of the load to be shed when applying the static sensitivity-based UFSL scheme detailed in [9] and the FRCC LS scheme [17]. These results are reported in Table V, which clearly shows that the proposed UFLS provides the minimum amount of LS for recovering the frequency very near to its nominal value.

Lastly, the proposal runs on an Intel® Core I5 2.40 GHz computer with 12 GB of RAM. In this context, Table VI reports the CPU times required for the different stages of the proposed approach when computing the sensitivities at t=t_{nss}. As expected, the sensitivity analysis required the most time during the frequency stabilization process, as reported in column 3.

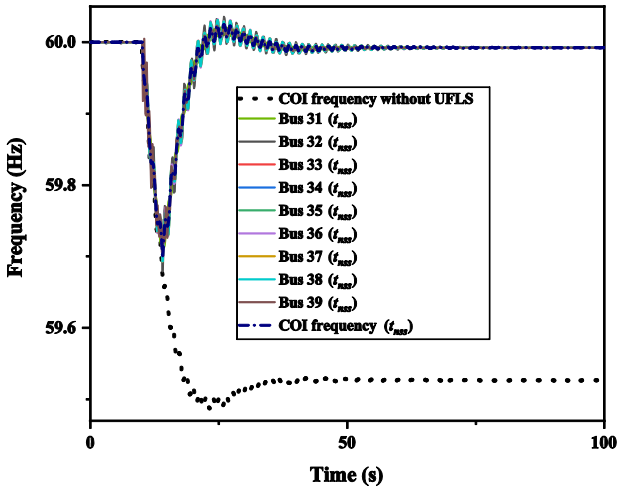

Figure 4. Frequencies for the New England 39-bus system for LS at t_{nss}.

D. *IEEE 118-bus system*

The proposed approach is applied to the IEEE 118-bus system composed of 19 generators, 35 synchronous condensers, 177 lines, 9 transformers, and 91 loads. The system data for the dynamic- and steady-state analyses are taken from [19] and [20], respectively. It is assumed that a generation outage occurred at bus 10, producing a loss of 450 MWs: 10.44% of the system's total active power generation. This contingency decreased the frequency to a steady-state value of 58.87 Hz, as shown in Figure 5. Hence, a UFLS scheme is designed considering a maximum nodal frequency deviation of Δf_{max}=0.7 Hz so that the UFLS control action is activated at a frequency value of 59.3 Hz with a time delay of 0.2s. Furthermore, $\Delta f_{\max}^{BS} = 0.2$ Hz and $\Delta f_{\max}^{RS} = 0.1$ Hz. The stabilization process required only two iterations of the bracketing stage. Following the recommendation given in [18], the dynamic sensitivities were computed at a time in which the frequency returns to a constant value: t_{nss}=50s. The vector $\Delta \boldsymbol{P}_{RD}$ computed from the sensitivity analysis indicates that all loads can be shed, with the loads embedded at buses 102 and 109 possessing a major impact on the stabilization process. The first iteration of the stabilization process results in a $f_{PI}(t_{nss})$=24.403 Hz and a total LS of 272.96 MW, which was applied at t_{LS}=1.8s to recover the frequency value of 59.49 Hz. Since this value is below 59.8 Hz, a second iteration was performed with a solution of $f_{PI}(t_{nss})$=4.876 Hz and a total amount of LS of 502.72 MWs:13.79% of the total load, where loads at buses 102 and 109 are shed in 15.21% and 15.31%, respectively. In this case, the generators' nodal frequencies and COI frequency evolved to a value of 60.03 Hz, as shown in Figure 5, so no refinement phase was needed.

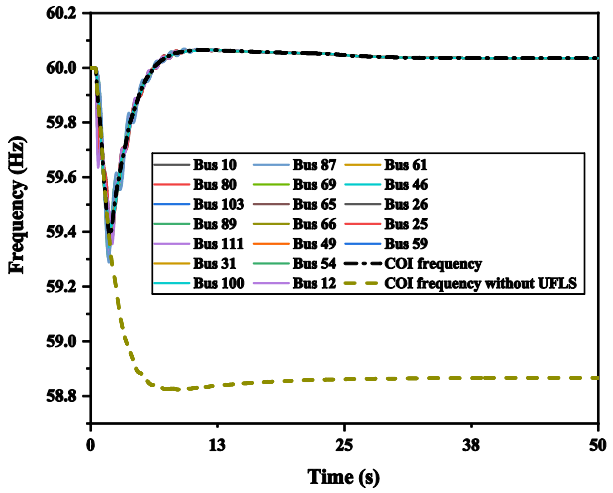

Figure 5. Frequency system without UFLS and with the proposed UFLS.

VII. CONCLUSIONS

This paper proposes a new frequency stability-constrained optimal LS that relies on the independent sequential solution of the frequency stability and optimal LS problems framed in a unified frame of analysis through a frequency performance index. Within this context, a systematic trajectory-based approach is derived from first principles to identify the most suitable loads to be shed in terms of their impact on improving the load-generation balance and, in turn, on the effectiveness of the control action without using heuristic criteria. Based on this sensitivity analysis, an optimization problem is formulated to determine how the UFLS control action must selectively perform the amount of LS for maintaining nodal frequencies within prescribed limits. The effectiveness of the proposed approach is successfully illustrated by numerical examples so that its practical application becomes attainable.

REFERENCES

[1] P. Kundur, J Paserba, V. Ajjarapu, G. Anderson, A. Bose, C. Canizares, N. Hatziargyriou, D. Hill, A. Stankovic, C. Taylor, T. Van Cutsem and V. Vittal, "Definition and classification of power system stability," *IEEE Trans. Power Syst.*, vol. 19, no. 3, pp. 1387–1401, 2004.

[2] X. Xu, H. Zhang, C. Li, Y. Liu, W. Li and V. Terzija, "Optimization of the Event-Driven Emergency Load-Shedding Considering Transient Security and Stability Constraints," *IEEE Trans. Power Syst*., vol. 32, no. 4, pp. 2581-2592, Jul. 2017.

[3] H. Golpîra, H. Bevrani, A.R. Messina, and B. Francois, "A data-driven under frequency load shedding scheme in power systems," *IEEE Trans. Power Syst*., vol. 38, no. 2, pp. 1138-1150, May 2022.

[4] V. V. Terzija and H. J. Koglin, "New approach of adaptive automatic load shedding," *Eur. Trans. Electr. Power*, vol. 11, no. 5, pp. 329–334, 2001.

[5] F. Ceja-Gomez, S. Qadri, and F. Galiana, "Under-frequency load shedding via integer programming," *IEEE Trans. Power Syst.*, vol. 27, no. 3, pp. 1387–1394, Aug. 2012.

[6] I. R. Fitri and J. S. Kim, "Priority-Considered Load Shedding in Economic Dispatch: Distributed Optimization Approach," *IEEE Trans. Control Netw. Syst*., vol. 10, no. 3, pp. 1400-1411, 2022.

[7] C. Wang, S. Chu, Y. Ying, A. Wang, R. Chen, H. Xu and B. Zhu, "Underfrequency Load Shedding Scheme for Islanded Microgrids Considering Objective and Subjective Weight of Loads," *IEEE Trans. Smart Grid*, vol. 14, no. 2, pp. 899–913, 2023.

[8] A. A. Girgis and S. Mathure, "Application of active power sensitivity to frequency and voltage variations on load shedding," *Electr. Power Syst. Res.*, vol. 80, no. 3, pp. 306–310, 2010.

[9] T. N. Le, H. A. Quyen, T. T. B. Phan, N. A. Nguyen, and T. P. Trieu, "Select Location for Load Shedding In Power System," in *Proc. 2018 4th International Conference on Green Technology and Sustainable Development, GTSD 2018*, pp. 13–17.

[10] L. Tang and J. McCalley, "Two-stage load control for severe under-frequency conditions," *IEEE Trans. Power Syst.*, vol. 31, no. 3, pp. 1943–1953, 2016.

[11] D. Pasiopoulou, E. O. Kontis, T. Papadopoulos, and G. K. Papagiannis, "Effect of load modeling on power system stability studies," *Electr. Power Syst. Res.*, vol. 207, pp. 1–11, Feb. 2022.

[12] E.A. Zamora-Cárdenas and C.R. Fuerte-Esquivel, "Multi-parameter trajectory sensitivity approach for location of series-connected controllers to enhance power system transient stability," *Elect. Power Sys. Res*., vol. 80, no. 9, pp. 1096-1103, Sep. 2010.

[13] A. Pizano-Martinez, C.R. Fuerte-Esquivel, E. Zamora-Cárdenas and J.M. Lozano-García, "Directional derivative-based transient stability-constrained optimal power flow," *IEEE Trans. Power Syst.*, vol. 32, no. 5, pp. 3415-3426, Sept. 2017.

[14] M. Sun, G. Liu, M. Popov, V. Terzija, and S. Azizi, "Underfrequency Load Shedding Using Locally Estimated RoCoF of the Center of Inertia," *IEEE Trans. Power Syst.*, vol. 36, no. 5, pp. 4212–4222, 2021.

[15] DSATools™ (2023), Dynamic Security Assessment Software. [Online] Available: https://www.dsatools.com/ (Accessed on 14 September 2023).

[16] M. A. Pai, *Energy Function Analysis for Power System Stability*, vol. 18, no. 2. New York: Springer, 1989. p. 240.

[17] Florida Reliability Coordinating Council Inc. (FRCC), "FRCC System Disturbance and Underfrequency Load Shedding Event Report," FRCC, Tampa, Florida, Tech. Rep. Oct. 2008.

[18] M. N. Acosta, C. Adiyabazar, F. Gonzalez-Longatt, M. A. Andrade, J. Rueda, E. Vazquez and J. M. Riquelme, "Optimal under-frequency load shedding setting at Altai-Uliastai regional power system, Mongolia," *Energies*, vol. 13, no. 20, pp. 5390-5408, Oct. 2020.

[19] University of Cyprus (2020), IEEE 118-bus modified test system. [Online] Available: https://www2.kios.ucy.ac.cy/testsystems/index.php/ieee-118-bus-modified-test-system/ (Accessed on 07 September 2023).

[20] Illinois Information Trust Institute (2023), IEEE 118-Bus System. [Online] Available: https://icseg.iti.illinois.edu/ieee-118-bus-system/ (Accessed on 07 September 2023).